JACC: CARDIOVASCULAR IMAGING VOL. 1, NO. 6, 2008
© 2008 BY THE AMERICAN COLLEGE OF CARDIOLOGY FOUNDATION
ISSN 1936-878X/08/$34.00
PUBLISHED BY ELSEVIER INC. DOI:10.1016/j.jcmg.2008.06.009

Magnetic Resonance Cardiac Vein Imaging

Relation to Mitral Valve Annulus and Left Circumflex Coronary Artery

Amedeo Chiribiri, MD,*† Sebastian Kelle, MD,‡ Uwe Köhler, PHD,‡
Laurens F. Tops, MD,§ Bernhard Schnackenburg, PHD,‖ Rodolfo Bonamini, MD,†
Jeroen J. Bax, MD,§ Eckart Fleck, MD,‡ Eike Nagel, MD, PHD*

London, United Kingdom; Torino, Italy; Berlin and Hamburg, Germany; and Leiden, the Netherlands

OBJECTIVES To evaluate in vivo anatomical relationships between the coronary sinus–great cardiac vein (CS–GCV), the mitral valve annulus (MVA), and left circumflex coronary artery (LCX) with cardiovascular magnetic resonance.

BACKGROUND The CS–GCV has become an anatomical structure of interest because it provides a way of access to the heart for a number of interventional procedures. Previous reports demonstrate that the postulated close anatomical proximity of the CS–GCV to the MVA does not always hold true in patients, both in autopsy specimens and in vivo by computed tomography.

METHODS In 31 participants (24 volunteers and 7 patients; 15 men; 42 ± 19 years), cardiovascular magnetic resonance was performed for noninvasive evaluation of the coronary sinus and of the coronary arteries using whole-heart imaging and intravascular contrast agents. Three-dimensional reconstructions, standard orthogonal planes, and unprocessed raw data were used to assess CS–GCV anatomy and its relation to the MVA and the LCX along their entire course.

RESULTS The CS–GCV was located behind the left atrium in all examined participants, at a minimum distance of 8.6 ± 3.9 mm from the MVA. In 80% of the participants, the LCX crossed the CS–GCV inferiorly, between the CS–GCV and the MVA. The CS–GCV and the LCX had a parallel course for 26.2 ± 23.0 mm, with great variability of location and length. In several participants, the CS–GCV had a long parallel course, but in other participants, the LCX crossed below the CS–GCV at a discrete point.

CONCLUSIONS In all participants, the CS–GCV coursed behind the left atrium rather than behind the MVA. In the majority of the participants, the LCX coursed between the CS–GCV and the MVA. These anatomical relationships should be kept in mind when referring a patient for interventional procedures requiring the access to the CS–GCV, and cardiovascular magnetic resonance might provide important information for the selection of candidates for these procedures. (J Am Coll Cardiol Img 2008;1: 729–38) © 2008 by the American College of Cardiology Foundation

From *King's College London BHF Centre of Research Excellence, Division of Imaging Sciences, St. Thomas's Hospital, King's College London, London, United Kingdom; †Department of Internal Medicine, University of Torino, Torino, Italy; ‡Department of Internal Medicine/Cardiology, Deutsches Herzzentrum Berlin, Berlin, Germany; §Department of Cardiology, Leiden University Medical Center, Leiden, the Netherlands; and ‖Philips Medical Systems, Hamburg, Germany. Financial support was received from the Department of Health via the National Institute for Health Research (NIHR) comprehensive Biomedical Research Centre award to Guy's & St Thomas' NHS Foundation Trust in partnership with King's College London and King's College Hospital NHS Foundation Trust. Dr. Chiribiri is supported by a scholarship from the Italian Society of Cardiology.

Manuscript received April 4, 2008; revised manuscript received June 13, 2008, accepted June 25, 2008.

The coronary sinus and the great cardiac vein (CS–GCV) have become anatomical structures of interest because they are used as an easy way of access to the heart for several different procedures, so as to reach the left ventricle with pacemaker leads or to administer retrograde cardioplegia or in a series of different electrophysiological interventional procedures (1,2). Recently, it has been proposed to use the CS–GCV to perform percutaneous mitral valve annulus annuloplasty (PMVA) in patients with functional mitral regurgitation (3,4). The close relationship between the CS–GCV, the left circumflex artery (LCX), which usually courses close to the CS–GCV, and the mitral valve annulus (MVA) is the anatomical substrate responsible for the efficacy of the procedure and could predict the complications already described during percutaneous procedures requiring access to the CS–GCV (5–7). Thus, the description of the anatomic relations between the CS–GCV, the MVA, and the LCX could be of great value in the selection of patients considered for these procedures.

Cardiac magnetic resonance (CMR) has become an important and sophisticated tool for noninvasive evaluation of the cardiovascular structures. Thus, the aim of this study was to evaluate the feasibility of CMR to depict the relation between the CS–GCV, the MVA, and the LCX.

ABBREVIATIONS AND ACRONYMS

CMR = cardiac magnetic resonance

CS–GCV = coronary sinus and the great cardiac vein

LCX = left circumflex artery

MVA = mitral valve annulus

PMVA = percutaneous mitral valve annulus annuloplasty

METHODS

Study population. We examined 31 participants (24 volunteers and 7 patients; 15 men; 41 ± 19 years) who received an intravascular contrast agent. Gadomer-17 (SH L 643A, Schering, Berlin, Germany) was used within a phase II study to evaluate the coronary arteries (7 patients and 8 volunteers), and gadofosveset (MS-325, EPIX Pharmaceuticals, Cambridge, Massachusetts, and Schering), now approved in many countries as Vasovist (Bayer Schering Pharmaceutical, Berlin, Germany), was also used within a phase I trial to evaluate the coronary arteries in the remaining 16 volunteers.

The inclusion criterion for the patients was suspected or known coronary artery disease with an indication for invasive angiography, without a history of coronary artery bypass grafting. The inclusion criterion for the volunteers was a low likelihood of coronary artery disease (<5% according to the Diamond and Forrester criteria). All participants included in the aforementioned trials at our center were included in the current retrospective analysis.

Participants with contraindications to CMR or history of an anaphylactic reaction to any allergen were excluded from the study. Patients were also excluded if they had atrial fibrillation or frequent ventricular extrasystoles.

The institutional review board approved the study protocol, and written informed consent was obtained from all participants.

Contrast agents. Gadomer-17 is a gadolinium-based intravascular contrast agent. It does not show considerable extravasation to the interstitial space (8). Every patient received a 0.15-mmol/kg body weight dose that was administered intravenously.

Vasovist is a gadolinium-based intravascular contrast agent recently approved for magnetic resonance angiography of the peripheral vascular system (9–11). Every volunteer received a 0.05-mmol/kg body weight dose that was administered intravenously.

Magnetic resonance imaging. All participants were examined using a whole body magnetic resonance system (Intera CV 1.5-T, Release 9, Philips, Best, the Netherlands) equipped with a power gradient system (33 mT/m, 160 T/m/s slew rate). A 5-element cardiac synergy coil was used for signal detection. Cardiac synchronization was performed using a vector electrocardiogram. For registration of diaphragmatic motion during free breathing a navigator (gating window: 6 mm) placed at the right dome of the diaphragm was used (12). Identification of the heart and diaphragm was done using a free-breathing multistack single-shot 2-dimensional balanced steady-state free-precession scan with transverse, sagittal, and coronal images of the thorax. This scan was required for placement of the navigator and planning of the sequences (13). A cine steady-state free-precession sequence with 50 heart phases was performed to determine the diastolic rest period of the coronary arteries.

The start of the acquisition as well as acquisition duration of the coronary angiography sequences was adapted to the patients' individual coronary artery rest period with a maximal acquisition time of 90 ms.

An inversion-prepared 3-dimensional steady-state free-precession balanced sequence with the following parameters was used 2 to 10 min after administration of the contrast agent: 110 to 130 transversal slices, repetition time/echo time/flip angle = 6.4 ms/3.2 ms/85°, fat suppression, SENSE

(sensitivity encoding; reduction factor 2). The measured voxel size was 1.18 × 1.18 × 1.18 mm^3 or lower, reconstructed to 0.7 × 0.7 × 0.9 mm^3 or better (up to 0.7 × 0.7 × 0.7 mm^3); the field of view was 340 × 340 mm; and the bandwidth was 560 Hz/pixel. Pre-pulse delay was individually determined with a Look-Locker sequence before the contrast-enhanced scan.

Image analysis. Data were analyzed on a post-processing workstation (Viewforum Release 4.2V1L2, Philips Medical Systems, Best, the Netherlands). A multiplanar curved reconstruction of the CS–GCV was obtained by the Soapbubble program (MR-Software/Pride, Philips Medical Systems), simultaneously displaying multiple vessels in a 2-dimensional representation (14).

ANATOMICAL AND QUANTITATIVE ANALYSES. Three-dimensional volume-rendered reconstructions and reconstructed standard long-axis 2-, 3-, and 4-chamber projections of the left ventricle were used to assess the position of the CS–GCV in relation to the MVA and the LCX with respect to the CS–GCV and their relative positions at their crossing point.

Reconstructed long-axis views in the 2-, 3-, and 4-chamber projections of the left ventricle were used to assess the course of the CS–GCV and to measure its diameters and the distance between the CS–GCV and the MVA, which is defined as the distance from the MVA plane to a parallel line drawn through the center of the CS–GCV (Fig. 1). The diameter of the MVA was measured in the same projections. The diameters of the CS–GCV were also measured at its ostium, which is defined as the site where the CS–GCV makes an angle with the right atrium.

The course of the LCX and the CS–GCV, the position of the MVA, the relative distance of the CS–GCV and MVA, the length of the vessels, the length of parallel course of the CS–GCV and the LCX, and the perimeter of the MVA were determined by manually tracking the center of each vessel and the points of insertion of the mitral valve leaflets on unprocessed raw data. Distances were measured by a specifically designed software tool that was created using Labview (National Instruments, Austin, Texas).

Statistical analysis. Continuous data are presented as mean values ± SD; categorical data are presented as frequencies and percentages. Differences between measurements were compared using *t* test for paired observations or using 1-way analysis of variance for repeated measurements. Differences between volunteers and patients were assessed by independent samples *t* test. All statistical analyses were performed using SAS System (version 9.1, SAS Institute, Cary, North Carolina). All statistical tests were 2-sided, whereas a p value <0.05 was considered significant.

RESULTS

In all participants, the CS–GCV was visible from its origin to the anterior interventricular vein. The

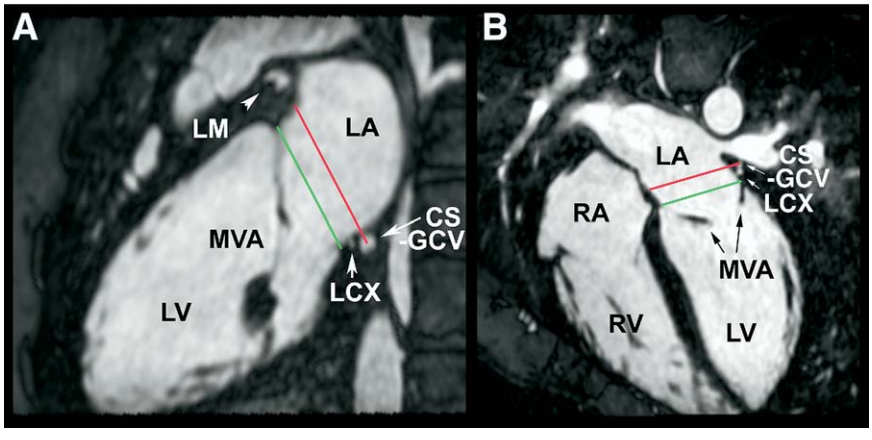

Figure 1. Multiplanar-Reformatted Views Representing the Constant Separation Between the MVA Plane and the CS–GCV

The 2-chamber **(A)** and 4-chamber **(B)** views show the measurements of the distance between the coronary sinus–great cardiac vein (CS–GCV) and the mitral valve annulus (MVA) plane **(green line)**. The **red line** represents a parallel line drawn through the center of the CS–GCV. LA = left atrium; LCX = left circumflex coronary artery; LM = left main coronary artery; LV = left ventricle; RA = right atrium; RV = right ventricle.

mean assessable length was 113.5 ± 14.8 mm (Table 1). The LCX was visible in 29 participants (93.5%), for a mean length of 60 ± 24 mm (Table 2). In all participants, it was possible to adequately track the insertion points of the mitral valve leaflets on the ventricular wall and on the subaortic septum.

CS–GCV diameters and MVA measurements. The diameter of the CS–GCV at the ostium and in the 2-, 3-, and 4-chamber views (Table 1) showed a significant decrease in mean size with increasing distance to the origin of the CS–GCV ($p < 0.001$ in both anteroposterior and superoinferior directions), and the diameter of the CS–GCV at the ostium and in the 4-chamber view was larger in patients than in volunteers (Table 3).

The diameter of the MVA was 39 ± 5 mm in the 2-chamber view, 36 ± 4 mm in the 3-chamber view, and 35 ± 4 mm in the 4-chamber view ($p < 0.001$) (Table 1), without a difference between volunteers and patients (Table 3). The mean perimeter of the MVA was 121 ± 15 mm.

In all participants, the CS–GCV was adjacent to the left atrial wall rather than to the MVA. The mean distance of the CS–GCV to the MVA was 11.1 ± 3.7 mm (range: 5 to 20 mm) in the 2-chamber view, 11.1 ± 3.9 mm (range: 4 to 22 mm) in the 3-chamber view, and 9.7 ± 3.1 mm (range: 4 to 18 mm) in the 4-chamber view, without any significant difference between the locations ($p = 0.11$).

Table 1. CS-GCV Diameter and MVA Measurements, Evaluated on Raw Unprocessed Data

Type of Measure	Measurement (mm)	p Value
CS-GCV evaluable length*	113.5 ± 14.8	0.96†
CS-GCV ostial diameter, anteroposterior; superoinferior	9.9 ± 4.3; 10.4 ± 4.8	
CS-GCV diameter, anteroposterior; superoinferior		
2-chamber view	7.4 ± 1.7; 8.3 ± 2.1	0.04†
3-chamber view	5.3 ± 1.3; 6.3 ± 2.6	0.13†
4-chamber view	5.2 ± 1.5; 5.5 ± 1.9	0.57†
MVA perimeter‡	121 ± 15	
MVA diameter		
2-chamber view	39 ± 5§	
3-chamber view	36 ± 4§	
4-chamber view	35 ± 4§	

*Range: 85 to 148. †$p < 0.001$ for the 1-way ANOVA comparison of CS-GCV diameter at the ostium and in 2-, 3-, and 4-chamber views. ‡Range: 80 to 140. §$p < 0.001$ for the 1-way ANOVA comparison of MVA diameter in 2-, 3-, and 4-chamber views.
ANOVA = analysis of variance; CS-GCV = coronary sinus–great cardiac vein; MVA = mitral valve annulus.

Table 2. Relationship of CS-GCV, LCX, and MVA

Type of Measure	Measurement (mm)	Range
LCX evaluable* length	60 ± 24	19–97
CS-GCV–MVA minimal distance	8.6 ± 3.9	2–15
LCX-MVA minimal distance	7.6 ± 3.1	3–13
CS-GCV–LCX minimal distance	2.7 ± 1.0	1–11
CS-GCV ostium to LCX cross length	71.5 ± 29.9	22–100
CS-GCV–LCX parallel course	22.6 ± 23.0	0–95
CS-GCV–MVA distance at LCX crossing	11.0 ± 4.8	2–21

*We were able to visualize and evaluate the LCX in 29 of 31 (93.5%) participants.
LCX = left circumflex artery; other abbreviations as in Table 1.

When comparing volunteers and patients, the mean distance between CS–GCV and MVA was significantly different only in the 4-chamber view, being 9 ± 3 mm for volunteers and 12 ± 4 mm for patients, $p = 0.008$ (Table 3). The minimal distance between the CS–GCV and the MVA along its full course was 8.6 ± 3.9 mm (range: 2 to 15 mm [Table 2]; 7.4 ± 3.3 mm for volunteers and 12.4 ± 3.3 mm for patients, $p = 0.001$ [Table 3]).

The 3-dimensional analysis of the MVA position in space confirmed that this anatomical structure is not located in 1 plane but has a saddle-shaped configuration extending to different planes (Fig. 2, Online Video 1) (15).

Relation between the coronary sinus, the LCX, and the MVA. The relation between the CS–GCV, the LCX, and the MVA are summarized in Table 2. The minimal distance of the LCX to the MVA was 7.6 ± 3.1 mm (range: 3 to 13 mm), without a difference between volunteers and patients (Table 3). In 2 participants, the LCX was not assessable. The LCX crossed between the CS–GCV and the MVA in 25 participants (80.6%), and in 4 participants, the LCX passed above the CS–GCV (12.9%). The minimal distance between the LCX and the CS–GCV was 2.7 ± 1.0 mm. The distance from the CS–GCV ostium to the LCX crossing was 71.5 ± 29.9 mm (range: 22 to 100 mm), without any difference between volunteers and patients. The distance between the CS–GCV and the MVA at the CS–GCV-LCX crossing point was 11.0 ± 4.8 mm (range: 2 to 21 mm), being 9.6 ± 3.8 mm for volunteers and 17.4 ± 3.6 mm for patients ($p < 0.001$) (Table 3).

The length of the overlap between CS–GCV and LCX was highly variable, with a mean parallel

Table 3. Comparison of Volunteers and Patients

Type of Measure	Chamber View	Volunteers (n = 24)	Patients (n = 7)	p Value
CS-GCV–MVA distance, mm	2C	11 ± 4	13 ± 4	0.2
	3C	11 ± 4	12 ± 5	0.5
	4C	9 ± 3	12 ± 4	0.008
CS-GCV–MVA minimal distance, mm		7.4 ± 3.3	12.4 ± 3.3	0.001
CS-GCV diameter, vertical; horizontal, mm	Ostium	7 ± 6; 7 ± 6	12 ± 4; 12 ± 3	0.02/0.03
	2C	8 ± 2; 7 ± 2	8 ± 1; 8 ± 5	0.1/0.4
	3C	6 ± 3; 5 ± 1	7 ± 3; 6 ± 2	0.5/0.02
	4C	5 ± 2; 5 ± 1	7 ± 2; 7 ± 2	0.01/0.005
MVA diameter, mm	2C	39 ± 5	39 ± 3	0.9
	3C	36 ± 3	36 ± 5	0.7
	4C	35 ± 3.9	37 ± 3	0.2
CS ostium to LCX cross length, mm		74 ± 22	74 ± 52 (n = 5)	0.4
CS-GCV–MVA distance at LCX crossing, mm		9.6 ± 3.8	17.4 ± 3.6 (n = 5)	<0.001
LCX-MVA minimal distance, mm		7.1 ± 3.0	9.4 ± 2.5	0.1
CS-GCV–LCX length of parallel course, mm		29 ± 23	29 ± 18 (n = 5)	0.2
MVA perimeter, mm		113 ± 13	123 ± 14	0.13

Abbreviations as in Tables 1 and 2.

course of 26.2 ± 23.0 mm (range: 0 to 95 mm). In several participants, the CS–GCV and the LCX had a long parallel course (Figs. 3A and 3B, purple line), also parallel to the MVA (Fig. 3B, yellow line). The distance between the CS–GCV and the LCX increased again at the anterior wall of the heart, where the CS–GCV turned toward the apex as an anterior interventricular vein. Conversely, in other participants, the LCX crossed below the CS–GCV at a discrete point (Fig. 3D), without any parallel course (Fig. 3E, purple line). In contrast, in these participants, the distance from the CS–GCV to the MVA remained constant (Fig. 3E, yellow line).

The overlapping segment of CS–GCV and LCX was <30 mm long in 18 participants (58.1%) or longer in 11 participants (35.5%). In 1 participant, it was possible to identify an anterior U-turn of the CS–GCV pathway around the LCX (Fig. 4A). Figure 4B shows an example of a 3-dimensional reconstruction of the posterior surface of the heart, demonstrating the position of the CS–GCV adjacent to the left atrium.

DISCUSSION

This study demonstrates the capability of CMR to evaluate noninvasively the anatomical relation between the CS–GCV, the MVA, and the LCX. All the CS–GCV, 94% of the LCX, and 100% of basic valvular anatomy could be assessed.

The major findings of the study are that the CS–GCV is located adjacent to the left atrial wall rather than at the level of the MVA and that in the majority of the participants, the LCX courses between the CS–GCV and the MVA. The relation between the CS–GCV and the LCX is highly variable in terms of distance, crossing point, and length of the parallel course. All these features can be evaluated noninvasively using CMR and should be taken into account when selecting patients for percutaneous procedures involving the CS–GCV.

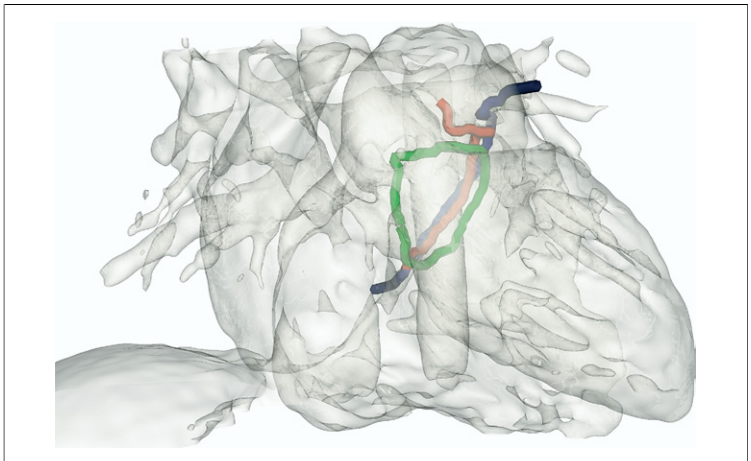

Figure 2. Transparent Reconstruction of the Heart Fused With the CS–GCV, the LCX, and the MVA

The CS–GCV is represented in **blue,** the MVA in **green,** and the LCX in **red**. The CS–GCV and the LCX show a long parallel course. The MVA shows the typical saddle shape. Abbreviations as in Figure 1. See Online Video 1.

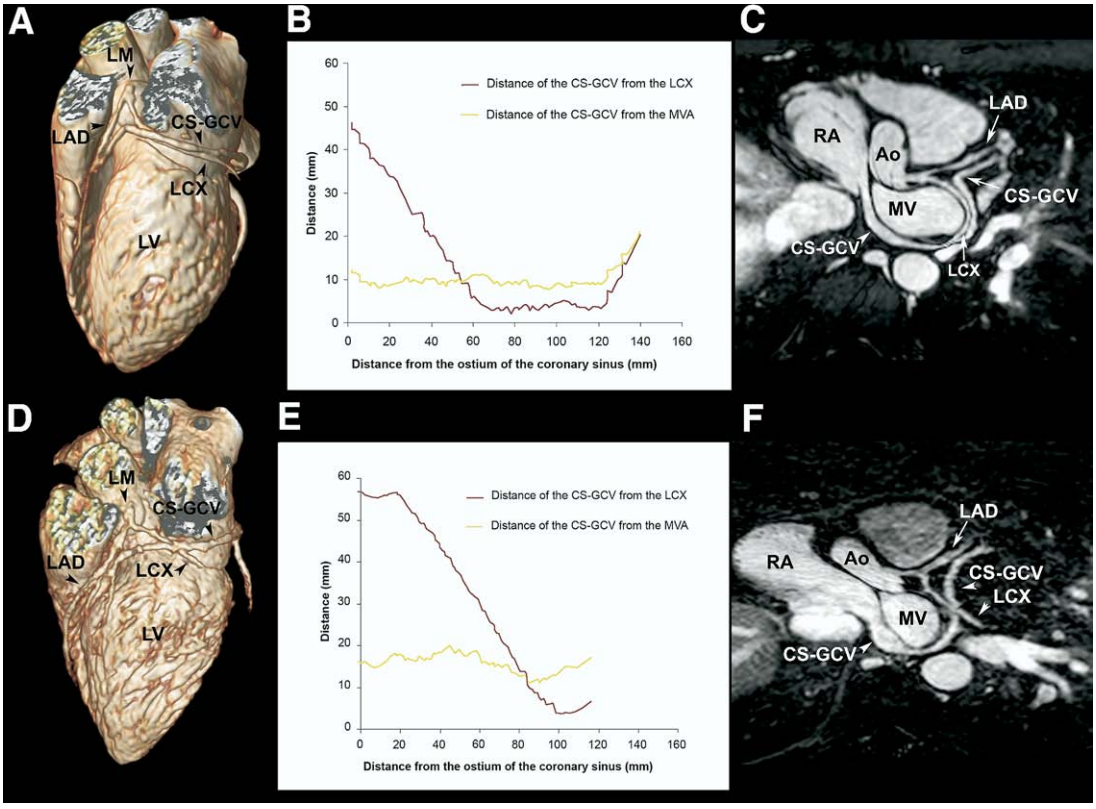

Figure 3. Three-Dimensional Representation and Measurements of the Anatomical Relationship Between the CS–GCV, the MVA, and the LCX Along Their Entire Course

(A) Three-dimensional reconstruction showing a case with a long parallel course of the CS–GCV and the LCX. **(B)** Distance between the CS–GCV and the closest point of the LCX **(purple line)**; distance between every point of the CS–GCV and the closest point of the MVA **(yellow line)**. **(C)** Curved multiplanar reformatting showing the LCX running parallel to the CS–GCV in the same participant. **(D)** Three-dimensional reconstruction showing a case with a discrete crossing of the LCX under the CS–GCV. **(E)** Distance between the CS–GCV and the LCX **(purple line)**; the distance of the CS–GCV from the MVA remains quite constant **(yellow line)**. **(F)** Curved multiplanar reformatting showing the LCX crossing down the CS–GCV in the same participant. Ao = ascending aorta; LAD = left anterior descending coronary artery; MV = mitral valve; other abbreviations as in Figure 1.

Anatomical and quantitative observations. The relations between the CS–GCV, the MVA, and the LCX were previously described in some anatomical studies (16–18). Several reports described the possibility of visualizing the venous system of the heart using computed tomography (19–21). The relations between the CS–GCV, the MVA, and the LCX were investigated noninvasively (22–24) (Table 4).

A constant separation exists between the CS–GCV and the MVA. In our study, the CS–GCV was always located adjacent to the left atrial wall rather than to the MVA, which agrees with the findings of previous studies (16–18,23,24) (Table 4).

Furthermore, we observed among patients a larger separation between the CS–GCV and the MVA in the 4-chamber view when compared with the separation in volunteers. These data confirm the results reported by Choure et al. (23), who found the same increase among patients with mitral regurgitation and suggested a possible flattening of the MVA saddle shape, which may result in a reduction of the forces for mitral valve leaflet closure (25). In our population, a larger diameter of the CS–GCV in this position may also have contributed to this result (Table 3).

The minimal distance of the CS–GCV along its course from the MVA has been previously reported (17,24). We confirmed that even the minimum distance of the CS–GCV from the MVA is not negligible, and we demonstrated that the minimal distance between the CS–GCV and the MVA was increased among patients.

Surprisingly, we found that the relation between the CS–GCV and the LCX was much closer than that between the CS–GCV and the MVA. In fact, the minimum distance of the CS–GCV along its

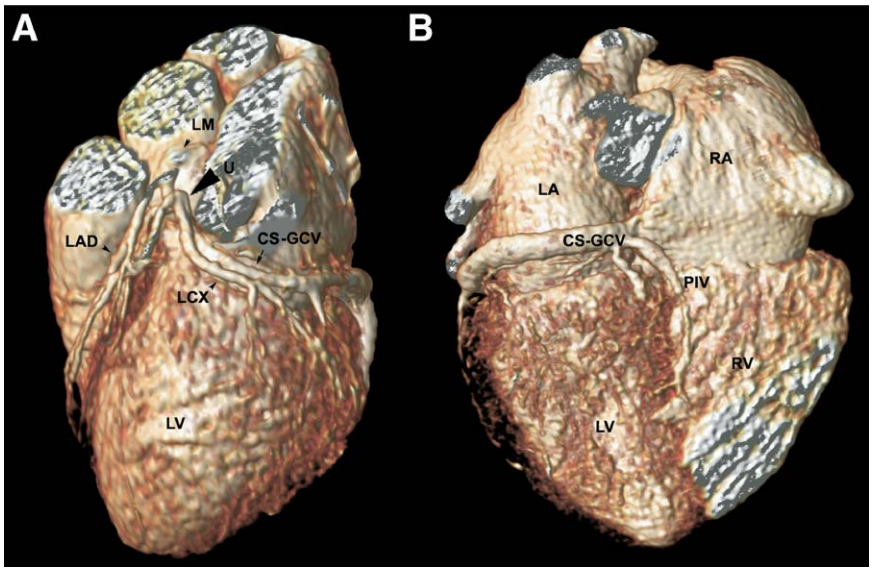

Figure 4. Three-Dimensional Reconstructions Showing the Anatomical Variability of the Relationships Between the Vascular Structures in the Atrioventricular Groove, and the Close Relationship Between the CS–GCV and the Left Atrial Wall

(A) Three-dimensional reconstruction (anterior view) showing the position of the CS–GCV and of the LCX, which makes a U-turn around the CS–GCV **(U)**. **(B)** Three-dimensional reconstruction (posterior view) showing the position of the CS–GCV, which is adjacent to the left atrial wall rather than the MVA. The coronary arteries have been removed for better visualization of the atrioventricular groove. PIV = posterior interventricular vein; other abbreviations as in Figures 1 and 3.

course from the LCX was 1.3 ± 1 mm in a previous study (24). We detected a small minimal distance between the CS–GCV and the LCX (2.7 ± 1 mm), confirming the tight relation between the CS–GCV and the LCX. Furthermore, the LCX crossed between the CS–GCV and the MVA in a large proportion of patients. We also carefully described the other characteristics of the relation between CS–GCV and LCX. In particular, the initial crossing point between the CS–GCV and the LCX was usually located in the lateral region of the heart, at a mean distance from the CS–GCV ostium of 71.5

Table 4. Summary of Data Available From Studies About the Anatomical Relation Between CS-GCV, MVA, and LCX

	Method	Number of Patients	CS-GCV Located Behind Left Atrium	CS-GCV–MVA Posterior Distance (mm)	Minimum CS-GCV–MVA Distance (mm)	Minimum CS-GCV–LCX Distance (mm)	LCX Between CS-GCV and MVA	CS-GCV–LCX Overlap >30 mm	Distance CS-Ostium to LCX Crossing (mm)	CS-GCV–MVA Distance at CS-GCV–LCX Crossing (mm)
Shinbane et al. (16)	Anat	10	100%	14.1 ± 3.1*	—	—	—	—	—	—
El-Maasarany et al. (17)	Anat	40	92.5%	9.4†	5.2 ± 1.6	—	95.2%	—	—	—
Maselli et al. (18)	Anat	61	100%	9.7 ± 3.2‡	—	—	69.3%	—	—	—
Mao et al. (22)	CT	231	—	—	—	—	80.8%	17.8%	—	—
Choure et al. (23)	CT	36	100%	10.4 ± 2.0§	—	—	80%	—	78.2 ± 18.7	8.0 ± 2.0
Tops et al. (24)	CT	105	90%	8.8 ± 2.3‖	5.1 ± 2.9	1.3 ± 1.0	68%	—	—	—
Chiribiri et al. (current study)	CMR	31	100%	11.1 ± 3.7§	8.6 ± 3.9	2.7 ± 1.0	80.6%	35.5%	71.5 ± 29.9	11.0 ± 4.8

*At 20 mm from CS ostium. †At 36° rotation from the CS ostium; ‡At P_3 scallop level of the mitral valve; §2-chamber view; ‖At "proximal CS."
Anat = anatomical dissection of human cadaver hearts; CS = coronary sinus; CT = computed tomography; CMR = cardiovascular magnetic resonance; other abbreviations as in Tables 1 and 2.

mm. The CS–GCV also was separated from the MVA at this level, with an increase of its diameter and distance among patients.

Moving from this point to the anterior side of the heart, the relation between the CS–GCV and the LCX showed 2 different patterns: in several patients, the 2 vessels coursed parallel for a long tract, but in others they crossed in a discrete point (Fig. 3). Previously, only 1 study (22) partially described this relation. Mao et al. (22) found a parallel course between the CS–GCV and the LCX longer than 30 mm in 17.8% of cases. In our study, it was possible to depict carefully the details of this anatomical relation. The length of the CS–GCV–LCX parallel course was highly variable, and we demonstrated that 35.5% of participants revealed a parallel course longer than 30 mm, with a high anatomical variability, suggesting an even tighter relation between the 2 vessels than has previously been reported.

Implications for PMVA. Even though highly attractive, PMVA might be applied only to a subset of patients, due to the mechanism of mitral valve regurgitation and the anatomical relations demonstrated by the current study (25) (Table 4). In fact, when the CS–GCV courses along the left atrial wall, PMVA may not be useful and might even alter the size and shape of the MVA in a negative manner (23), resulting in a mitral annular deformation through secondary tension effects from the left atrial wall and leading to suboptimal results (25). Furthermore, although the venous system in all participants crossed from the atrial side of the MVA to the ventricular side, this always happened in a discrete point and was different from what happened with the CS–GCV–LCX crossing point, which was represented by a parallel course at least in a subgroup of the participants.

Another potential concern with CS–GCV device implantation is the compression of the coronary arteries, and LCX compression has been reported during PMVA in both human and animal studies (26). Not all of these crossovers will necessarily result in coronary artery flow reduction (25), but the variability of the relation between the CS–GCV and the LCX demonstrated by our study may result in an important technical limitation of PMVA (27). Further studies will be needed to ascertain whether the risk of LCX compression is higher when the LCX crosses inferior to the CS–GCV and over a large distance (Fig. 3).

In previous studies, the CS–GCV coursed adjacent to the MVA in only a small subset (0% to 9% of patients) (16,18,23,24), and the LCX did not cross under the CS–GCV in a minority of patients, varying from 4.8% to 30.7% (17,18). The PMVA devices might also displace rather than compress the LCX. Furthermore, the distance of the CS–GCV–LCX crossing point from the CS–GCV ostium could be of great importance in selecting patients for whom PMVA might be useful, as the mitral annular size needs to be decreased by 20% to 30% to achieve a significant reduction in mitral regurgitation (3). This reduction could not be possible in patients with the vessels crossing within 75% of the proximal end of the coronary sinus (3).

The anatomy of the CS–GCV, MVA, and LCX needs to be assessed before considering PMVA. Whenever possible, this evaluation should be performed noninvasively to determine whether a transvenous approach for the reduction of mitral regurgitation is feasible. The present study demonstrates for the first time that CMR is capable of a complete evaluation of the relevant anatomical features of the region (25). The main advantage of CMR, besides its safety profile, is flexibility with respect to the anatomical needs. Computed tomography requires the use of X-rays and iodine contrast agents and uses rectangular data acquisition. Conversely, CMR does not require the use of radiation, is considered a safe procedure, and is more flexible and close to the anatomical situation because of its multidimensional capability. Only a small number of papers have been published (28–30) about possible serious side effects of gadolinium contrast agents in patients with end-stage chronic renal disease.

Study limitations. In this study, we evaluated participants without heart failure. Whether these findings are reproducible in dilated hearts, and in patients with a left ventricular ejection fraction lower than 35% who could be the target of PVMA, remains to be demonstrated. Furthermore, we retrospectively analyzed participants who were originally enrolled in clinical studies to evaluate intravascular contrast agents for coronary artery imaging. All the sequence parameters, the timing for image acquisition, and the dosages of the contrast agent were decided on the basis of the original study design. The administration of the intravascular contrast agents, regardless of the type used, made it possible to visualize the CS–GCV and the LCX in all but 2 participants. Nezafat et al. (31) examined different technical modalities to improve CMR vein imaging and discussed the differences between systolic and diastolic image acquisition and different types of sequence. We retrospectively analyzed datasets acquired to evaluate the coronary arteries, choosing a

diastolic timing. This approach has several advantages: the diastolic resting period is usually longer than the systolic resting period, making identification easier and image acquisition faster, which reduces cardiac motion-related image blurring. Nezafat et al. (31) showed that the diameter of the cardiac veins changes during the heart cycle, and the maximum diameter occurs in the end-systolic phase. However, the choice of the end-diastolic quiescent phase did not affect the meaning of our study, because the CS–GCV was completely visualized in all the participants. Furthermore, the CS–GCV was always located in correspondence with the atrial wall rather than at the level of the MVA. We expect a systolic increase of the distance of the CS–GCV from the MVA, depending on the increase in the diameter of the left atrium during the systole.

Nezafat et al. (31) compared different types of sequences, demonstrating the best image quality when using magnetization transfer preparation instead of no preparation or T_2-preparation of the contrast. Further studies are needed to determine the best approach in a clinical setting.

CONCLUSIONS

The present study shows the feasibility of CMR to depict the CS–GCV anatomy and its relation to the MVA and LCX. An accurate selection of potential candidates for interventions requiring access to the CS–GCV is needed, and CMR can provide the required anatomical information.

Reprint requests and correspondence: Prof. Dr. Eike Nagel, King's College London, Division of Imaging Sciences, The Rayne Institute, 4th Floor Lambeth Wing, St. Thomas's Hospital, London SE1 7EH, United Kingdom. *E-mail: eike.nagel@kcl.ac.uk*

REFERENCES

1. Gaita F, Riccardi R, Caponi D, et al. Linear cryoablation of the left atrium versus pulmonary vein cryoisolation in patients with permanent atrial fibrillation and valvular heart disease: correlation of electroanatomic mapping and long-term clinical results. Circulation 2005;111:136–42.
2. Jais P, Hocini M, Hsu LF, et al. Technique and results of linear ablation at the mitral isthmus. Circulation 2004;110:2996–3002.
3. Duffy SJ, Federman J, Farrington C, Reuter DG, Richardson M, Kaye DM. Feasibility and short-term efficacy of percutaneous mitral annular reduction for the therapy of functional mitral regurgitation in patients with heart failure. Catheter Cardiovasc Interv 2006;68:205–10.
4. Webb JG, Harnek J, Munt BI, et al. Percutaneous transvenous mitral annuloplasty: initial human experience with device implantation in the coronary sinus. Circulation 2006;113:851–5.
5. Morady F, Strickberger A, Man KC, et al. Reasons for prolonged or failed attempts at radiofrequency catheter ablation of accessory pathways. J Am Coll Cardiol 1996;27:683–9.
6. Pappone C, Oral H, Santinelli V, et al. Atrio-esophageal fistula as a complication of percutaneous transcatheter ablation of atrial fibrillation. Circulation 2004;109:2724–6.
7. Takahashi Y, Jais P, Hocini M, et al. Acute occlusion of the left circumflex coronary artery during mitral isthmus linear ablation. J Cardiovasc Electrophysiol 2005;16:1104–7.
8. Herborn CU, Barkhausen J, Paetsch I, et al. Coronary arteries: contrast-enhanced MR imaging with SH L 643A—experience in 12 volunteers. Radiology 2003;229:217–23.
9. Parmelee DJ, Walovitch RC, Ouellet HS, Lauffer RB. Preclinical evaluation of the pharmacokinetics, biodistribution, and elimination of MS-325, a blood pool agent for magnetic resonance imaging. Invest Radiol 1997;32:741–7.
10. Bluemke DA, Stillman AE, Bis KG, et al. Carotid MR angiography: phase II study of safety and efficacy for MS-325. Radiology 2001;219:114–22.
11. Grist TM, Korosec FR, Peters DC, et al. Steady-state and dynamic MR angiography with MS-325: initial experience in humans. Radiology 1998;207:539–44.
12. Jahnke C, Paetsch I, Nehrke K, et al. Rapid and complete coronary arterial tree visualization with magnetic resonance imaging: feasibility and diagnostic performance. Eur Heart J 2005;26:2313–9.
13. Prakken NH, Vonken EJ, Velthuis BK, Doevendans PA, Cramer MJ. 3D MR coronary angiography: optimization of the technique and preliminary results. Int J Cardiovasc Imaging 2006;22:477–87.
14. Etienne A, Botnar RM, Van Muiswinkel AM, Boesiger P, Manning WJ, Stuber M. "Soap-Bubble" visualization and quantitative analysis of 3D coronary magnetic resonance angiograms. Magn Reson Med 2002;48:658–66.
15. Salgo IS, Gorman JH III, Gorman RC, et al. Effect of annular shape on leaflet curvature in reducing mitral leaflet stress. Circulation 2002;106:711–7.
16. Shinbane JS, Lesh MD, Stevenson WG, et al. Anatomic and electrophysiologic relation between the coronary sinus and mitral annulus: implications for ablation of left-sided accessory pathways. Am Heart J 1998;135:93–8.
17. El-Maasarany S, Ferrett CG, Firth A, Sheppard M, Henein MY. The coronary sinus conduit function: anatomical study (relationship to adjacent structures). Europace 2005;7:475–81.
18. Maselli D, Guarracino F, Chiaramonti F, Mangia F, Borelli G, Minzioni G. Percutaneous mitral annuloplasty: an anatomic study of human coronary sinus and its relation with mitral valve annulus and coronary arteries. Circulation 2006;114:377–80.
19. Jongbloed MR, Lamb HJ, Bax JJ, et al. Noninvasive visualization of the cardiac venous system using multislice computed tomography. J Am Coll Cardiol 2005;45:749–53.
20. Gerber TC, Sheedy PF, Bell MR, et al. Evaluation of the coronary venous system using electron beam computed tomography. Int J Cardiovasc Imaging 2001;17:65–75.

21. Van de Veire NR, Schuijf JD, De Sutter J, et al. Non-invasive visualization of the cardiac venous system in coronary artery disease patients using 64-slice computed tomography. J Am Coll Cardiol 2006;48:1832–8.
22. Mao S, Shinbane JS, Girsky MJ, et al. Coronary venous imaging with electron beam computed tomographic angiography: three-dimensional mapping and relationship with coronary arteries. Am Heart J 2005;150:315–22.
23. Choure AJ, Garcia MJ, Hesse B, et al. In vivo analysis of the anatomical relationship of coronary sinus to mitral annulus and left circumflex coronary artery using cardiac multidetector computed tomography: implications for percutaneous coronary sinus mitral annuloplasty. J Am Coll Cardiol 2006; 48:1938–45.
24. Tops LF, Van de Veire NR, Schuijf JD, et al. Noninvasive evaluation of coronary sinus anatomy and its relation to the mitral valve annulus: implications for percutaneous mitral annuloplasty. Circulation 2007;115: 1426–32.
25. Piazza N, Bonan R. Transcatheter mitral valve repair for functional mitral regurgitation: coronary sinus approach. J Interv Cardiol 2007;20: 495–508.
26. Maniu CV, Patel JB, Reuter DG, et al. Acute and chronic reduction of functional mitral regurgitation in experimental heart failure by percutaneous mitral annuloplasty. J Am Coll Cardiol 2004;44:1652–61.
27. Feldman T, Glower D. Patient selection for percutaneous mitral valve repair: insight from early clinical trial applications. Nat Clin Pract Cardiovasc Med 2008;5:84–90.
28. Grobner T. Gadolinium—a specific trigger for the development of nephrogenic fibrosing dermopathy and nephrogenic systemic fibrosis? Nephrol Dial Transplant 2006;21: 1104–8.
29. Dharnidharka VR, Wesson SK, Fennell RS. Gadolinium and nephrogenic fibrosing dermopathy in pediatric patients. Pediatr Nephrol 2007;22:1395.
30. Broome DR, Girguis MS, Baron PW, Cottrell AC, Kjellin I, Kirk GA. Gadodiamide-associated nephrogenic systemic fibrosis: why radiologists should be concerned. AJR Am J Roentgenol 2007;188:586–92.
31. Nezafat R, Han Y, Peters DC, et al. Coronary magnetic resonance vein imaging: imaging contrast, sequence, and timing. Magn Reson Med 2007; 58:1196–206.

Key Words: intravascular contrast agents ■ mitral valve annulus ■ coronary sinus ■ left circumflex coronary artery ■ mitral valve repair ■ magnetic resonance imaging

APPENDIX

For an accompanying video and legend, please see the online version of this article.